

# CONFINEMENT IN TOKAMAKS

J.ONGENA

Laboratoire de Physique des Plasmas-Laboratorium voor Plasmafysica  
Association "Euratom-Etat belge"-Associatie "Euratom-Belgische Staat"  
Ecole Royale Militaire-Koninklijke Militaire School  
Brussels

## I. INTRODUCTION

The total amount of heating power coupled to the plasma  $P_{tot}$  and the energy confinement time are determining parameters for realizing the plasma conditions suitable for the reactor. We recall that the ignition condition can be expressed by the following condition on the triple fusion product:

$$nT\tau = \frac{P_{tot} \tau^2}{3Vol} = \frac{3n^2 T^2 Vol}{P_{tot}} > (nT\tau)_{ignition} \quad (1)$$

where  $\tau = E / P_{tot}$  is the energy confinement time,  $E = 3nT Vol$  for an isothermal plasma with  $T_i = T_e = T$  and a plasma volume  $Vol$ ;  $n$  is the plasma density. The value  $T \approx 15 \text{ keV}$  corresponds to the minimum value of  $(n\tau T)_{ignition}$  as a function  $T$  (see Fig. 1). In the present discussion for the sake of simplicity, we neglect density and temperature profile factors. The heating power in most of the present experiments is given by  $P_{tot} = P_{OH} + P_{add}$  where  $P_{OH}$  is the ohmic power and  $P_{add}$  is the additional heating due to neutral beam injection or radiofrequency heating. At ignition, the additional heating power must come completely from the energetic  $\alpha$ -particles produced by the fusion reactions and we must have  $P_{tot} = P_\alpha$  if we neglect the residual  $P_{OH}$  and the plasma losses by Bremsstrahlung ( $P_{Br} \propto n^2 \sqrt{T}$ ).

Around  $T \approx 15 \text{ keV}$  the fusion power  $P_f$  is approximately given by:

$$P_f = 5P_\alpha \propto n^2 T^2 Vol \propto \beta^2 B_t^4 \quad (2)$$

This expression shows that for a given machine characterised by his volume and toroidal magnetic field  $B_t$  i.e. his cost, the achieved value of  $P_f$  depends on the plasma beta

$$\beta = 4 \mu_0 \frac{nT}{B_t^2} = 0.01 \beta_n \frac{I_p}{aB_t}$$

The value of  $\beta$  is generally normalised with respect to the ratio  $\frac{I_p}{aB_t}$  expressed in MA/(m T) (where  $I_p$  is the plasma current and  $a$  is the plasma minor radius) which is an important parameter to express the beta limit of the toroidal plasma due to MHD instabilities; the achieved beta performances of a given machine are then expressed by the factor  $\beta_N$ . The fusion power is limited by the maximum achievable value of  $\beta_N$  through the relation

$$P_{f,max} \propto \beta_n^2 \left( \frac{I_p}{aB_t} \right)^2 Vol B_t^4 \propto \left( \frac{\beta_n}{q} \right)^2 \left( \frac{a}{R} \right)^2 Vol B_t^4 \quad (3)$$

where  $q$  is the discharge safety factor at the edge  $q = \frac{5a^2 B_t}{RI_p}$  (m,T,MA), and  $R$  is the major radius.

In the present machines with negligible fusion power production,  $\beta_N$  and  $\tau$  are also determining the maximum heating power, given by the formula below, that the discharge can tolerate without disruption due to the  $\beta$  limit:

$$P_{tot,max} = 0.0375 \frac{\beta_{n,max}}{\mu_0 \tau q} B_t^2 \left( \frac{a}{R} \right) Vol \quad (4)$$

Equ. (4) is generally a non-linear equation in  $P_{tot}$  because  $\tau$  is a function of  $P_{tot}$  (e.g.  $\tau \propto P_{tot}^{-0.5}$ ).

In a reactor operating at  $T \approx 15 \text{ keV}$ , the maximum beta and therefore the maximum fusion power can also be limited by the maximum achievable plasma density. For gas puff fuelled discharges it is found empirically that the maximum observed density in a tokamak is the so-called Greenwald limit [1] given by:

$$\bar{n}_{eo,GR} = \frac{I_p}{\pi a^2} = \frac{5B_t}{\pi Rq} \quad (10^{20}m^{-3}, MA, m, T) \quad (5)$$

when expressed in the mentioned units,  $\bar{n}_{eo,GR}$  being the central line averaged density. The ratio  $\bar{n}_{eo} / \bar{n}_{eo,GR}$  is often called the Greenwald number and its value thus indicates how close a given plasma density is with respect to the Greenwald limiting density. Note that in the last 2 years several machines have overcome this limit to a large extent and have obtained Greenwald factors of up to 1.7 stationary and up to 2 transiently. In most of the cases these supra-Greenwald densities are accompanied by a strong reduction in confinement, even lower than L-Mode confinement (see § II.A for a discussion of the different confinement modes). Under RI-Mode conditions as obtained on TEXTOR (see § IV.B), this degradation in confinement can be overcome and discharges can be obtained with a Greenwald factor of 1.4 with simultaneously ELM-free H-Mode confinement.

In the original design of ITER (International Thermonuclear Experimental Reactor) as specified in the Final Design Report [2,15] the following values for the machine parameters are considered:  $R = 8.14$  m,  $a = 2.8$  m (with elongation  $\kappa \sim 1.6$ ),  $B_t = 5.68$ T,  $I_p = 21$  MA,  $P_f = 1.5$  GW,  $n\tau T = 3.3 \times 10^{21} m^{-3} keV s$ ,  $\bar{n}_{eo} = 1.3 \times \bar{n}_{eo,GR}$ ,  $\beta_N = 2.4$ ,  $\tau = 6$ s,  $E = 1.2$  GJ. Note that the current design of ITER (2009) is one with reduced parameters, (caused by the withdrawal of the US as an ITER partner in 1996 for a mix of political and erroneous scientific reasons; they joined again in 2001). The current ITER design (2009) has a 50% reduced capital cost compared to the previous larger design and the main parameters are:  $R = 6.2$ m,  $a=2.0$ m,  $\kappa=1.70-1.85$ ,  $B_t = 5.3$ T,  $I_p = 15-17$ MA,  $P_f = 500-700$ MW,  $\bar{n}_{eo} = \bar{n}_{eo,GR}$ ,  $\beta_N = 1.8 - 2.4$ ,  $\tau = 3.6-3.9$ s.

To reach ignition, the ohmic power alone is not sufficient and additional heating power is necessary. Additional heating of tokamak plasma is performed by neutral beam injection and radio-frequency heating. Various ranges of frequencies are used for the radio-frequency heating. Mainly (i) the ion cyclotron frequency range (ICRH  $\sim 10$  to  $150$  MHz) where powerful tetrodes are used as power source and where electron and ion heating is possible; (ii) the lower hybrid frequency range (LH  $\sim 1$  GHz to  $10$  GHz) which is used mainly for current drive (LHCD) and where the power is delivered by klystrons; (iii) the electron cyclotron frequency range (ECRH  $\sim 30$  to  $200$  GHz) where electron heating is performed and which uses gyrotrons as power source. This last frequency band requires the simplest structures inside the tokamak achieving the highest RF power density but still requires the development of gyrotrons able to deliver long pulses in the MW range to compete with the ICRH method. ICRH together with neutral beam

injection are the most widely used methods for additional heating on large machines.

## II.CONFINEMENT IN OHMIC AND ADDITIONALLY HEATED DISCHARGES WITHOUT INTERNAL TRANSPORT BARRIER

### II.A. Scaling laws

Confinement in tokamak plasmas does not behave classically due to anomalous diffusion. There exist many theoretical models of anomalous diffusion linked to different types of turbulence which can be classified in two main categories: electrostatic and magnetic turbulence. Each theory leads to its own expression for the scaling of confinement. Up to now, the major mechanism(s) for anomalous diffusion have not been clearly identified. In practice, empirical scaling laws are derived by assuming that the global confinement scaling can be taken as a power law of so-called engineering quantities:

$$\begin{aligned} \tau &= C_1 I_p^\mu R^\rho a^\alpha B_t^\beta n^\nu P_{tot}^\pi \kappa^k M_i^\mu \\ &= C_2 a^{2+\alpha} B_t^{1+\beta} n^\nu P_{tot}^\pi R^{\rho-1} q^{-1} \kappa^k M_i^\mu \end{aligned} \quad (6)$$

(where  $M_i$  is the ion atomic mass and  $\kappa = b/a$  the plasma elongation) and by fitting this expression to an as large as possible set of experimental data obtained on different tokamaks.

Note (i) that the engineering quantities can be replaced by a set of non-dimensional ones which are assumed to express the physics of confinement (e.g.  $\rho^*$ ,  $\beta$ ,  $v^*$ ,  $a/R$ ,  $\kappa$ ,  $q$ ,  $M_i$ ) [3] and (ii) that other expressions can be considered to fit to the confinement database (as e.g. the linear offset scaling: see § II.B).

### II.B. Confinement scaling of ohmically and additionally heated tokamaks

Following the presentation of B.B.Kadomtsev [4] the usual confinement of ohmic and additionally heated discharges can be summarised as following (see Fig. 2):

(A) In ohmically heated discharges, at low plasma densities, the energy confinement is proportional to the plasma density and can be expressed by the so-called Neo-Alcator or Linear Ohmic Confinement (LOC) scaling law (here given for the circular case i.e.  $\kappa = 1$ ):

$$\tau_{NA} \propto \bar{n}_{eo} R^2 a q^\alpha M_i^{0.5} \quad (7)$$

where  $\bar{n}_{eo}$  is the central line-averaged density,  $R$  and  $a$  resp. the major and minor radius. We added a

dependence on the atomic mass  $M_i$  of the plasma ions which is often observed [5];  $q$  is the safety factor at the edge with  $0.5 < \alpha < 1.0$ , depending on the machine. For TEXTOR it has been shown [6] that  $0.5 < \alpha < 0.8$  and for the sake of simplicity, we take  $\alpha = 0.5$ . The Neo-Alcator scaling is considered as the experimental optimal mode for confinement in tokamaks [4]. Above a certain density  $n_s$ , a saturation of the ohmic confinement can occur. This Saturated Ohmic Confinement regime (also called SOC) has a low density dependence and can often be described by taking the L-mode scaling law for additional heated discharges (see equation (8) in the next section), where  $P_{tot}$  is substituted by the ohmic heating power,  $P_{OH}$  [7].

Using an adequate procedure for the conditioning of the wall [8] or pellet injection it is possible to restore a Neo-Alcator scaling for confinement at high densities. This regime, which has been called Improved Ohmic Confinement (IOC) is the prolongation of  $\tau_{NA}$  above  $\bar{n}_{e0} = n_s$  as shown in Fig. 2. Practically, on TEXTOR at high densities, the ohmic confinement lies between  $\tau_{NA}$  and  $\tau_{SOC}$  depending upon the machine condition.

	$C_1$	$\nu$	$\rho$	$\alpha$	$\beta$	$\nu$	$\pi$	$k$	$\mu$
GOLDSTON [9]	$3.68 \times 10^{-2}$	1.00	1.75	-0.37	0.00	0.00	-0.50	0.50	0.50
KAYE-GOLDSTON [10]	$3.02 \times 10^{-2}$	1.24	1.65	-0.49	-0.09	0.26	-0.58	0.28	0.50
ITERL-89P [11]	$4.80 \times 10^{-2}$	0.85	1.20	0.30	0.20	0.10	-0.50	0.50	0.50
ITERL-97P [12]	$3.40 \times 10^{-2}$	0.96	1.89	-0.06	0.03	0.40	-0.73	0.64	0.20
ITERH-92P(Y) [13]	$3.40 \times 10^{-2}$	0.90	1.90	-0.20	0.05	0.30	-0.65	0.80	0.40
IPB98(y,2) [14]	$3.65 \times 10^{-2}$	0.93	1.39	0.58	0.15	0.41	-0.69	0.78	0.19
ITERH-93P [15]	$3.60 \times 10^{-2}$	1.06	1.90	-0.11	0.32	-0.17	-0.67	0.66	0.41
ITERH-97P [16]	$3.10 \times 10^{-2}$	0.95	1.84	0.08	0.25	0.35	-0.67	0.63	0.42

Table I: Coefficients for confinement scaling expressions of the form

$$\tau = C_1 I_p^\nu R^\rho a^\alpha B_i^\beta n^\nu P_{tot}^\pi \kappa^k M_i^\mu$$

with units (s, MA, m, m, T,  $10^{19} \text{m}^{-3}$ , MW, -, -)

(B) When additional heating is applied, the basic mode of confinement is L-mode. If one looks at the values of the exponents for different empirical scalings (see Table I), one observes that to a good approximation:

$\nu \cong 1$ ,  $\beta \cong 0$ ,  $\nu \cong 0$ ,  $\alpha \cong 0$ ,  $\rho \cong 1.5$ ,  $\pi \cong -0.5$ ,  $k \cong 0.5$ ,  $\mu \cong 0.5$   
Therefore Equ. (6) can be approximated as :

$$\tau = f_H C_1 I_p R^{1.5} P_{tot}^{-0.5} (\kappa A_i)^{0.5} \quad (8)$$

where  $f_H$  is an enhancement factor with respect to the considered scaling. It is characterised by a low-density dependence, a linear increase with current and a degradation with the total applied heating power.

Illustrations of the low-density dependence and of the power degradation of the L-mode are given on Figs. 3a and 3b.

The L-mode scaling can also be described approximately by the T-10 scaling ([4], p.141):

$$\tau_{T-10} = \tau_{SOC} \sqrt{\frac{P_{OH}}{P_{tot}}} \cong \tau_L \quad (9)$$

Many improved confinement schemes have roughly the same parametric dependence, and can be characterised by their enhancement factor  $f_H$  with respect to L-mode scaling. The best known is the H-mode regime, for which  $f_H = 1.5$  to 2 (see the ITERH-93P scaling of Table I for ELM-free H-mode discharges which has a parametric dependence similar to the L-mode scalings).

The H-mode is an improved confinement regime which is observed in divertor machines above a certain threshold for the additional heating power. The H-Mode is characterised by the following features: existence of a transition between the usual confinement regime (L-mode) and the H-mode with a reduction of the  $H_\alpha$  light at the transition, formation of a density and/or temperature pedestal at the plasma edge and an improvement of the energy and particle confinement time. During the H-mode, MHD events called ELMs (Edge Localised Modes) can occur and the confinement improvement will depend on their repetition rate. Moreover, at high density a further degradation is often observed, and it is difficult to maintain the H-mode or even L-mode confinement up to the density limit of the machine (cfr. the discussion of the Greenwald limit in § I).

The largest confinement is obtained in the absence of ELMs but this confinement regime leads to non-stationary discharges ending with the onset of MHD phenomena and with a tendency of impurity accumulation in the centre of the plasma (see Fig. 4a). Stationary conditions can be obtained in ELMy H-Mode discharges (see Fig. 4b). Confinement in such plasmas is somewhat lower than in ELM-free H-Modes and can be roughly characterised by:

$$\tau_{ELMy H-mode} = 0.85 \times \tau_{ITERH-93P} \quad (10)$$

The ELMy H-mode regime is presently considered as the favourite operational regime for ITER to reach ignition.

The extrapolation of ELMy H-Mode confinement, as given by equation (10), to the parameters of ITER is shown in Fig. 5.

Additionally heated discharges can also be described, especially for the transition from OH to predominantly additionally heated conditions, by the

linear offset scaling [6]:

$$\tau_{OL} = \frac{\tau_{OH} P_{OH} + \tau_{inc} (P_{tot} - P_{OH})}{P_{tot}} \quad (11)$$

with  $\tau_{OH}$  being the ohmic confinement time and equal to  $\tau_{NA}$  or  $\tau_{SOC}$ , depending on the machine conditions. The incremental confinement time  $\tau_{inc}$  is proportional to  $I_p$  [6] and is relatively insensitive to  $P_{tot}$  and  $\bar{n}_{e0}$  for not too high values of these quantities. At high values of  $P_{tot}$ ,  $\tau_{inc}$  decreases as given by Equ (8). Fig. 6a shows the evolution of  $E = P_{tot} \tau_{OL}$  as a function of  $\bar{n}_{e0}$  compared to the behaviour of the ohmic energy  $E_{OH} = P_{OH} \tau_{OH}$ . For  $\bar{n}_{e0} > n_s$  the increase in plasma energy,  $\tau_{inc} (P_{tot} - P_{OH})$ , can take place with respect to the Neo-Alcator scaling (or its extension above  $n_s$ , IOC) instead of the SOC. Starting from SOC, one would find an apparent large  $\tau_{inc}^*$  (see Fig. 6a). In fact, the total increase of energy is not only due to the heating effect (as described by  $\tau_{inc}$ ) but also by the restoration of the non-saturated ohmic confinement regime by the additional heating (e.g. by its action on the plasma boundary) [6]. This is illustrated in Fig. 6b.

### II.C. Triple fusion product scaling

From equations (8) and (1) one can derive an approximate expression for the triple fusion product:

$$nT\tau = C_2 \left( \frac{f_H}{q} \right)^2 (aB_i)^2 M_i = C_3 \left( \frac{R}{a} I_p \right)^2 f_H^2 M_i \quad (12)$$

where  $f_H$  is the enhancement factor of the considered discharge regime with respect to a standard L or H mode scaling. The constants  $C_2$  and  $C_3$  depend on the scaling chosen.

Expression (12) shows that the value of the triple fusion product required for ignition  $(n\tau T)_{ignition}$  is more easily obtained at a large current and aspect ratio  $R/a$ , and with a large enhancement factor  $f_H$ . For a given value of  $aB_i$  (characterising the toroidal field coils) the ignition condition is strongly dependent on the ratio  $f_H/q$  which is considered as a figure of merit for ignition margin [8].

Equation (12) also shows that the usual power degradation observed for confinement  $\propto P_{tot}^{-0.5}$  leads to a scaling of the triple fusion product independent of the additional heating power.

Fig. 1 shows the values obtained for  $n\tau T$  versus  $T$  in different experiments. The ‘parabolic’ lines indicate the domains corresponding to ignition (reactor conditions) or breakeven (fusion power  $\equiv$  additional power supplied to the plasma).

## III. PLASMA THERMALISATION

For fusion reactions to occur, the kinetic energy of the ions has to be sufficiently large. The amount of energy transferred to ions and electrons depends on the heating method. Heating methods that deliver mainly energy to the plasma ions, can lead to the formation of energetic ion tails.

With neutral beam injection energetic ion beams are injected into the plasma. These beams have slowing down times proportional to  $\frac{T_e^{1.5}}{n_e}$  [17]. An

equal amount of energy is transferred from this energetic ion beam to the plasma ions and electrons if the beam energy  $E_b$  equals the so-called critical energy  $E_c \propto T_e$  [17]. For  $E_b > E_c$  the beam energy is predominantly delivered to the electrons. The  $\alpha$ -particles produced in fusion reactions mainly heat the electrons because their large energy (3.5 MeV) is much higher than  $E_b$ . The various heating scenarios used for ICRH heating (minority heating, wave conversion, ion harmonic cyclotron damping) often lead to the formation of hot energetic ion tails, and depending on the conditions the heating power is shared differently between plasma electrons and ions [17]. The fusion reactions due to the presence of ion energetic tails or beams can generate an appreciable part of the total fusion power, due to head-on collisions of the fast ions with slower or counter circulating fast ions (originating from counter beam injection). This is the case for tritium or deuterium neutral beam injection in a D-T plasma. The fusion power is then due to thermal, beam-target, and beam-beam reactions (see also § IV.C).

The ratio of the ion and electron thermal energy  $E_i$  resp.  $E_e$  can be derived from the energy balance equation of

(i) the total energy  $E = E_e + E_i$

$$\frac{dE}{dt} + \frac{E}{\tau} = P_{OH} + P_{add} = P_{tot} \quad (13)$$

where the global energy confinement time  $\tau$ , takes into account the losses due to conduction, convection, radiation and charge exchange,

(ii) the electron energy

$$\frac{dE_e}{dt} + \frac{E_e}{\tau_e} = P_{OH} + P_{add,e} - P_{e,i} \quad (14)$$

and (iii) the ion energy

$$\frac{dE_i}{dt} + \frac{E_i}{\tau_i} = P_{add,i} + P_{e,i} \quad (15)$$

where  $\tau_e$  and  $\tau_i$  are respectively the electron and ion confinement time and  $P_{e,i}$  is the power transferred from electrons to ions through Coulomb collisions. From (8) and (9) we have

$$\frac{I}{\tau} = \frac{I}{\tau_e} \frac{E_e}{E} + \frac{I}{\tau_i} \frac{E_i}{E} \quad (16)$$

In stationary conditions one can easily derive from Equations (14) and (15) the ratio between  $E_e$  and  $E_i$ . Taking into account that  $P_{e,i}$  can be expressed as  $\frac{(E_e - E_i)}{\tau_{equi}}$  where  $\tau_{equi}$  is an effective equipartition

time between the electrons and ions due to Coulomb collisions, we have:

$$\frac{E_i}{E_e} = \frac{P_{OH} + P_{add,e} + P_{add,i}(1 + \tau_{equi}/\tau_e)}{P_{add,i} + (P_{OH} + P_{add,e})(1 + \tau_{equi}/\tau_i)} \quad (17)$$

$\tau_{equi}$  is proportional to  $\frac{T_e^{1.5} M_i}{n_e Z_{eff}}$  where  $M_i$  is the ion atomic mass number and  $Z_{eff}$  is the effective charge of the ions of the plasma.

When  $\tau_{equi}$  is small with respect to  $\tau_e$  and  $\tau_i$  (i.e. at sufficiently high plasma density), we have a thermal plasma with  $E_e = E_i = \frac{1}{2} E$  and Equ. (16) becomes:

$$\tau = 2(\tau_e^{-1} + \tau_i^{-1})^{-1} \quad (18)$$

Note also that at high density the presence of energetic tails in the plasma becomes negligible and they thus contribute only to a small extent to the total plasma energy. Operational regimes with a (much) larger ion temperature than electron temperature are called "hot-ion modes".

#### IV. CONFINEMENT RESULTS IN PRESENT TOKAMAKS

In this section some recent some more details on recent confinement results are summarised. In Sect. 2.3 we indicated that a burning D-T fusion reactor, where the plasma heating is performed by the energetic  $\alpha$ -particles produced in the fusion reactions, requires a sufficiently large confinement time (expressed by  $f_H/q$  and a sufficiently large  $\beta$  (expressed by  $\beta_N/q$ ). A large  $\beta$  is achieved at a sufficiently large plasma density i.e. at a sufficiently large Greenwald number.

In addition, these requirements have to be fulfilled in stationary conditions with a low central pollution of the D-T plasma by impurities or ash (i.e.  $\alpha$ -particles) from the fusion reactions. This last condition is equivalent with requiring a sufficiently low He particle confinement. The heating power delivered to the plasma by the  $\alpha$ -particles will finally reach the walls of the machine and must then be evacuated. Without special precautions, this power will lead to a too large power flux in hot spots, resulting in large localised erosion or sputtering of the limiter or the divertor plates. Attempts are presently made to solve this problem by radiating homogeneously a large part of this power either in the plasma edge or in the divertor region, thus reducing to a serious extent the peak heat load values to the first wall.

In the next paragraphs a summary is given of different tokamak scenarii. They are presently under investigation to check their ability to simultaneously (i) reach high values for  $f_H$  and  $\beta_N$  (ii) solve the heat exhaust problem (iii) reach stationary conditions and (iv) to show evidence of plasma heating by  $\alpha$ -particles in D-T plasmas.

##### IV.A. H-mode discharges

Confinement characteristics of the H-Mode regime are summarised in § II.B. Fig. 4a shows an ELM-free H-mode discharge in JET that has led to a record neutron yield in D-D plasmas. This mode of operation is non-stationary and is limited in time by the occurrence of MHD phenomena (specifically for the discharge shown in the last figure: onset of MHD turbulence followed by a giant ELM). The ELMy H-mode regime is the favoured operational scenario for ITER because of its stationarity and good confinement characteristics (i.e. a sufficiently large  $f_H$ ). An example of such a discharge is shown in Fig. 4b [18]. Current investigations of this regime are related to its applicability to a reactor; more specifically (i) to reduce the uncertainty concerning the threshold heating power which has to be exceeded in the reactor to obtain the transition from L to H mode (ii) to try to obtain this regime at sufficiently large densities (equal to or above the Greenwald density, without loss of the good confinement properties) (iii) to solve the problem of heat exhaust, particularly in the presence of large ELMs. A way to solve this last problem is to seed impurities to produce edge radiation.

Recent experiments at JET [28, 29] have shown that it is possible to reach the ITER operational data for density and confinement simultaneously with (a) increasing the triangularity of the plasma, (b) by impurity seeding in low and high triangular plasmas and (c) by an adapted pellet fuelling cycle. Triangularity of a plasma can be roughly described as the "pointedness" of the plasma, and one

distinguishes in principle an upper  $\delta_U$  and lower  $\delta_L$  triangularity (Fig. 4c). Very often only the average triangularity  $\delta = (\delta_U + \delta_L)/2$  of the plasma is used. High triangularity is beneficial to increase confinement at high densities, as shown in Fig. 4d. These discharges are also quite robust to strong gas puffing (needed to reach the high density), provided sufficient heating power to keep Type I ELMs [30, 31]. The amount of power needed increased with decreasing triangularity. On the other hand, in low triangularity discharges high confinement and high density can be reached simultaneously by applying Ar seeding, as illustrated in Fig. 4e. This discharge shows a so-called "puff" and "after-puff" phase. In the puff phase strong gas puff is applied to raise the density to values around the Greenwald limit, but confinement degrades. This is restored in the afterpuff phase, i.e. when the strong gas puff is suddenly interrupted, and where only a gentle D and Ar puffing is continued, to keep density and radiation high. An adapted pellet fuelling cycle, where first a fast pellet train enters the plasma, followed by a second much slower pellet train (Fig. 4f), allows to reach high densities without degrading confinement too much. The philosophy here is much similar to the one applied in the low triangularity discharges with puff and afterpuff: first build up the density (irrespective of other quantities) and later on try to keep the high density without degradation of confinement, by a much gentler fuelling procedure.

#### IV.B. Discharges with edge radiation cooling and improved confinement

At a large radiated power fraction  $\gamma$ , it has been possible to achieve improved L-mode conditions with a confinement quality close to or even exceeding that of ELM-free H-mod [23]. In the next section examples of this regime are discussed.

A new confinement regime [24] has been established on TEXTOR-94, a tokamak with a circular cross-section and equipped with a toroidal pump limiter. This regime is obtained by appropriate impurity seeding during the heating phase of the discharge and has been called the Radiative I-mode (or RI-mode). It is characterised by its ability to simultaneously realise the following features, important for the extrapolation to a reactor: (i) quasi-stationarity of the plasma parameters, (ii) high confinement with a quality close to that of the ELM-free H-mode, (iii) high plasma density near or even above the Greenwald limit, (iv) high normalised beta ( $\beta_N$  up to 2), (v) strong edge radiation ( $\gamma = \frac{P_{rad}}{P_{tot}}$  up to 95 % where  $P_{rad}$  is the edge radiated power) (vi) the possibility to operate at low edge q values (down to 2.8), leading to reactor relevant values of the figure of merit for ignition  $f_H / q$ , (vii) no decrease of the plasma fusion reactivity due to the seeded impurity.

An example of the quasi-stationarity achieved in the RI-Mode is shown by the discharge in Fig. 7 which has

a high confinement phase of more than 7s, limited only by technical constraints of the machine. Remarkable in this figure is the evolution of the diamagnetic plasma energy  $E_{dia}$  and of the associated enhancement factor  $f_{H93}$ , which compares the experimentally obtained energy confinement time versus ELM-free H-mode confinement as given by the scaling law ITERH-93P (see Table I). Soon after the start of Ne seeding a confinement transition takes place, when  $\gamma \approx 50\%$ , resulting in a sudden increase of  $E_{dia}$  and  $f_{H93}$ . Note the long duration of the high confinement phase which is about 160 confinement times ( $\tau_E \approx 50\text{ms}$ ) and equivalent to several skin resistive times. We remark in passing that the ratio of the burn time to the projected confinement time of ITER (Final Design Report [25]) is also equal to 160! Note also that improved confinement at these high densities is not due to fast particle contributions (because of the high density reached) confirmed by the comparison of the measurements of the MHD  $E_{MHD}$  and diamagnetic energy  $E_{dia}$ .

The energy confinement in the RI-Mode improves with density and thus shows a totally different density behaviour as the usual L- or H-mode. This is illustrated in Fig. 8, where the evolution of  $E_{dia}$  is plotted versus  $\bar{n}_{eo}$  for ohmic discharges and discharges heated by the combination of NBI-co+ICRH with  $P_{tot} \approx 2.25$  MW at  $I_p = 350$  kA. The diamagnetic energy in ohmic discharges follows the Neo-Alcator scaling  $E_{NA}$  until  $\bar{n}_{eo} \approx 3.0 \times 10^{19} \text{m}^{-3}$  where a saturation sets in. For additionally heated discharges at low densities,  $E_{dia}$  follows roughly the L-mode scaling, or can be described by a linear offset scaling  $E_{OL} = E_{NA} + \tau_{inc}(P_{tot} - P_{OH})$  where  $P_{OH}$  is the ohmic heating power taken in a corresponding ohmic discharge and  $\tau_{inc}$  is the incremental confinement time, which is roughly constant for not too high  $P_{tot}$  or  $\bar{n}_{eo}$  and for a given  $I_p$ . A clear confinement transition occurs at  $\bar{n}_{eo} \approx 4.0 \times 10^{19} \text{m}^{-3}$ , where the  $E_{dia}$  values obtained differ substantially from L-mode scaling, resulting in a  $\tau_{inc}$  which increases strongly with density for  $\bar{n}_{eo} > 4.0 \times 10^{19} \text{m}^{-3}$ , as shown in Fig. 9. Discharges corresponding to these conditions belong to the RI-Mode, and are obtained as soon as  $\gamma$  exceeds about 50%. Furthermore, if  $f_{H93}$  values are plotted as a function of  $\bar{n}_{eo} / \bar{n}_{eo,GR}$  (for different plasma currents and for a wide range of  $P_{tot}$  and  $\gamma$ ) we find [24] not only that (i)  $f_{H93}$  increases approximately linearly with density but moreover that (ii) this result is independent of the plasma current. Therefore, the confinement time in RI-Mode discharges  $\tau_{RI}$  is proportional to  $(\bar{n}_{eo} / \bar{n}_{eo,GR}) \times \tau_{ITERH93-P}$ . A detailed analysis shows that the proportionality factor is close to 1 and we have thus to a very good approximation that:

$$\tau_{RI} = \frac{\bar{n}_{eo}}{\bar{n}_{eo,GR}} \times \tau_{ITERH93-P} \quad (19)$$

Striking in this formula is the linear density dependence (as for the ohmic Neo-Alcator scaling) and the absence of a current dependence, contrasting with the usual scalings for additionally heated discharges. The comparison of the global confinement time of the RI-mode with the L- and the ohmic LOC-regimes is shown in Fig. 2b. As low edge q operation ( $q_a = 2.8$ ) presents no stability problems, this leads then in a natural way to high values for the figure of merit for ignition margin  $f_{L89}/q_a$  equal to 0.65 at high density which is the value requested for the reactor. One still has to demonstrate that this regime can maintain its interesting features on larger and reactor size machines without significant central plasma pollution by the seeded impurity.

Confinement of the RI-Mode can be conveniently compared with confinement in the L- and H-Mode regime, independent of heating power or plasma current, in a normalised confinement diagram. Instead of plotting the confinement time  $\tau$  versus density (see e.g. Fig. 2a and 2b), one plots the quantity  $\tau P^{1.5}/I_p$  versus the Greenwald factor  $\bar{n}_{eo}/\bar{n}_{eo,GR}$ . The effect of such a transformation of variables is graphically depicted in Fig. 10b. The resulting diagram for RI-Mode data is given in Fig. 10c. One sees very clearly the L- and RI-Mode part in the data. One also sees that at the highest densities, RI-Mode confinement supersedes H-Mode confinement.

Discharges with a radiative mantle have now also been obtained at JET, with good confinement and density values using Ar as seeding impurity, as indicated in the previous section. A summary of main latest results obtained on JET can be found in [26]. Non noble gas impurities have been used ( $N_2$ ), leading to Type III discharges with rather small ELMs, but with degraded density (compared to the Greenwald density  $\bar{n}_{eo}/\bar{n}_{eo,GR}$ ) and confinement ( $f_{H93} \approx 0.7$ ).

#### IV.C. D-T operation

A preliminary D-T fusion experiment has been performed on JET in 1991 in plasmas with a mix of 10%D and 90%T [27] resulting in a fusion power output of about 1.7MW. In the period end 1993-beginning 1997, TFTR has been routinely operated with D-T discharges [28]. The operational regime in the high performance D-T discharges in TFTR was a (limiter) hot ion mode ( $T_{i0} > T_{e0}$ ) and was obtained with NBI heating, consisting of a mix of tritium and deuterium injection (to provide the necessary tritium fuelling of the discharge), resulting in a maximum fusion output of 10.7 MW. A second D-T experimental campaign has been performed in JET in September-November 1997. ELM-free H-Mode hot-ion modes,

optimised shear regimes and steady-state ELMy H-modes were used, heated by NBI or NBI combined with ICRH [29], again with part of the injectors being operated with tritium in order to provide at the same time the T fuelling. These experiments have resulted in the demonstration of near-break-even conditions:  $Q = P_{fusion}/P_{heating} = 0.62$  transiently, with an output power from fusion reactions of more than 16 MW; under quasi-stationary conditions  $Q = 0.35$  was obtained with a fusion power of about 5 MW. Fig. 11a gives a summary of the JET high performance D-T results and compares them to the results obtained previously on TFTR. Fig. 11b shows the time traces of the electron and ion temperatures of the record D-T fusion shot of JET. Maximum temperatures obtained for ions and electrons are resp. 28 keV and 14 keV. Fig. 11c shows the time trace of the different contributions to the neutron production as modelled by TRANSP [30]. This shot was heated by 22.3MW NBI and 3.1MW of ICRH. The total heating power in this discharge is also in part (about 3MW or nearly 10%) delivered by the  $\alpha$  particles generated in the fusion reactions. Note that the largest part of the fusion power output is due to reactions of thermal neutrons, with the rest mainly produced in beam-target reactions and only a small fraction due to beam-beam reactions. Due to their large energy the  $\alpha$  particles deposit their energy mainly to the electrons. Most of the ion heating is produced by the NBI and the largest part of the electron heating is due to the equipartition power between the hotter ions and the electrons. Note that for an ignited reactor the total heating power must be produced by the fast  $\alpha$  particles. These experiments have nevertheless demonstrated the effectiveness of  $\alpha$ -particle heating without significant plasma micro-instabilities.

Combined NBI-ICRH heating of D-T plasmas has also been performed on TFTR (and also recently on JET [31]) with direct heating of T ions at the second harmonic frequency for tritium  $2\omega_{CT}$ . A small amount (2 %) of  $^3He$  was added to the discharge to increase the single pass absorption by  $^3He$  minority heating [18]. In these experiments  $T_{i0}$  was increased from 26 to 36 keV and  $T_{e0}$  from 8 to 10.5 keV by the addition to 23 MW NBI of 5.5 MW of ICRH.

#### IV.D. Improved confinement through the formation of an Internal Transport Barrier (ITB)

After the L- to H-mode transition, the improvement in confinement is due to the formation of a transport barrier at the edge of the plasma [32] attributed to a transport reduction through ExB velocity shear decorrelation of the turbulence [32]. The VH-mode regime is linked to the penetration of the transport barrier deeper into the plasma.

ExB shear decorrelation of micro-instabilities (as e.g. in ITG modes) is not the only mechanism

which decreases transport. A reduction of transport (e.g. by reduction of MHD modes) is also possible by choosing an adequate value of the magnetic shear  $s = \frac{r}{q} \frac{dq}{dr}$ . Such confinement improvement schemes

are obtained by tailoring the current density resulting in

(i) discharges with a high internal inductance  $I_j$  (obtained e.g. by realising a highly peaked current density profile)

(ii) discharges with negative central magnetic shear i.e. with  $s = \frac{r}{q} \frac{dq}{dr} < 0$  in the centre of the plasma

resulting in a non-monotonic q-profile. The q value on the magnetic axis in that case is not the minimum q value in the q(r) profile. Such reversed shear plasmas are obtained in the presence of large non-inductive currents (bootstrap current, non-inductive current drive by e.g. LH) or by heating the plasma during the initial current ramp of the discharge. The formation of the Internal Transport Barrier (ITB) is due to a synergetic effect of transport reduction through adequate magnetic shear and ExB shear.

An example of a discharge on DIII-D with an ITB inside the plasma obtained with this last technique is shown in Fig. 12a. The minimum q is off-axis and the value for the safety factor in the centre of the plasma  $q_0$  is much larger than 1. A large confinement improvement is observed at the step in the neutral beam power, as evidenced by a large increase in the central  $T_j$  together with a peaking of the density profile. The effect of the formation of an ITB on the ion temperature profile of JET is shown in Fig. 12b.

The problem to extrapolate such these regimes to a reactor is to realise it in steady state and at sufficiently high density. An example of the achievement in TORE SUPRA [34] of a steady-state confinement improvement attributed to the presence of a large bootstrap current  $I_{BS}$  is shown in Fig. 13. The figure shows also the profile of the bootstrap current density profile and the obtained scaling of

$$I_{BS} \propto I_p \beta_p \sqrt{\frac{a}{R}} = q_a \beta_N I_p \sqrt{\frac{R}{a}} \quad (20)$$

## REFERENCES

- [1] M. Greenwald, J.L. Terry et al., Nucl. Fusion **28**, 2199 (1988).
- [2] "Technical basis for the ITER interim design report, cost review and safety analysis" ITER EDA documentation series n° 7, IAEA, Vienna, 1996.
- [3] J.G. Cordey, B. Balet et al., Plasma Physics Control. Fusion **38**, A67-A75 (1996).
- [4] B.B. Kadomtsev, "Tokamak Plasma : a complex physical system", Plasma Physics Series, IOP Publishing Ltd, Bristol and Philadelphia, 1992, pp 100-101.
- [5] F. Wagner, U. Stroth, Plasma Physics Control. Fusion **35**, 1321 (1993).
- [6] R.R. Weynants, Control. Fusion and Plasma Physics (Proc. 14th Eur. Conf. Madrid, 1987), **11D**, Part I, EPS, Geneva (1987) 197.
- [7] G. Bracco, K. Thomsen, Report JET-R(96)03 (1996).
- [8] M. Bessenroth-Weberpals, et al., Report MPI-IPP Garching 1/248 (1989).
- [9] R.J. Goldston, Plasma Physics and Control. Fusion **26** (1984) 87.
- [10] S.M. Kaye and R.J. Goldston, Nucl. Fusion **25** (1985) 65.
- [11] P.N. Yushmanov et al., Nucl. Fusion **30** (1990) 1999
- [12] S.M. Kaye and the ITER Confinement Database Working Group, Nucl. Fusion **37** (1997) 1303.
- [13] O.Kardaun and the ITER H-Mode Database Working Group, Plasma Physics and Controlled Nuclear Fusion Research (Proc 14<sup>th</sup> Int. Conf. Würzburg.1992) Vol 3 (Vienna:IAEA) 251.
- [14] ITER Expert Working Groups and the ITER JCT and Home Teams, *ITER Physics Basis Document*, Nucl. Fusion, **39**, 2137 (1999)
- [15] D.Schissel and the H-Mode Database Working Group (Proc. 20th EPS Conf. Lisbon (1993)) Vol 17C (1993), Part I, 103; K.Thomsen, Nucl. Fusion **34** (1994) 131.
- [16] Cordey J.G. and the ITER Confinement Database Working Group, Plasma Phys. Control. Fusion **39** (1997) B115.
- [17] See presentations by E.Lerche and D.Van Eester, these proceedings.
- [18] JET Team, in Plasma Physics and Control. Fusion, Nuclear Research 1997, IAEA Vienna, in print, paper IAEA-CN-64/01-4
- [19] J.Ongena et al, Plasma Physics Control. Fusion, **43**, A11-A30 (2001)

- [20] W.Suttrop et al., Phys. Plasmas **9** 2103 (2002)
- [21] G.Saibene et al, Proc. EPS Conference Funchal (Madeira), 18-24 June 2001
- [22] R.Sartori et al., Proc. EPS Conference on Plasma Physics and Controlled Fusion, Funchal (Madeira) 18-24 June 2001.
- [23] J. Neuhauser et al., Plasma Physics Control. Fusion **37** (1995) A37.
- [24] A.M. Messiaen, J. Ongena et al., Phys. Plasmas **4**, 1690 (1997).
- [25] Technical Basis for the ITER Final Design Report, ITER Documentation Series 15 and 16 (IAEA, Vienna, 1998)
- [26] J.Ongena et al., Fusion Science and Technology, **53**, No 4, 891 (2008).
- [27] JET Team, Nuclear Fusion **32** (1992) 187.
- [28] D.W. Johnson et al., Plasma Physics Control. Fusion **37** (1995) A69.
- [29] J.Jacquinot and the JET team, Plasma Physics Control. Fusion, **41** (1999) A13
- [31] JET Team, in Control. Fusion and Plasma Physics (Proc. 24th Eur. Conf. Berchtesgaden 1997), **21A**, Part IV, EPS, Geneva (1997) 1865.
- [32] K.H. Burrell, Phys. Plasmas **4** (1997) 1499.
- [33] S. Allen and R.A. Moyer, private communication.
- [34] Tore Supra Team, Plasma Phys. Control. Fusion **38** (1996) A251.

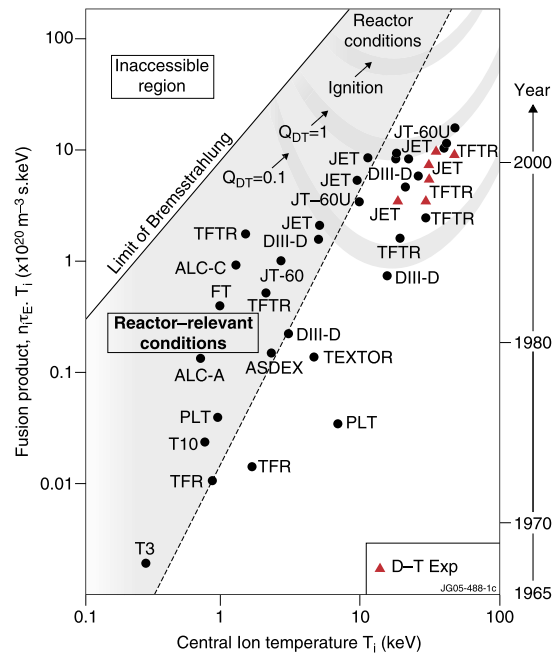


Fig. 1: Fusion triple product achieved in different tokamaks as a function of the ion temperature. The breakever  $Q = P_f / (P_{tot} - P_r) = 1$  and the ignition regions are shown. In the inaccessible region the Bremsstrahlung radiated power is too large and in the reactor relevant region we have  $T_i \ll T_e$  ( $eq \ll \ll$ )

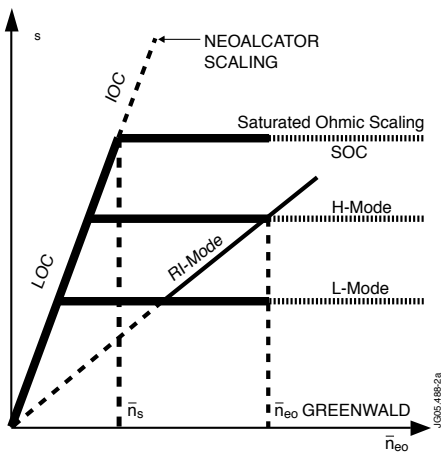


Fig. 2a: Schematic representation of the energy confinement time as a function of the density for ohmic discharges (at constant  $I_p$  and  $B_t$ ) and for additionally heated discharges (at constant  $I_p$ ,  $B_t$  and  $P_{tot}$ ) in the L-, H- and RI-Mode regime.

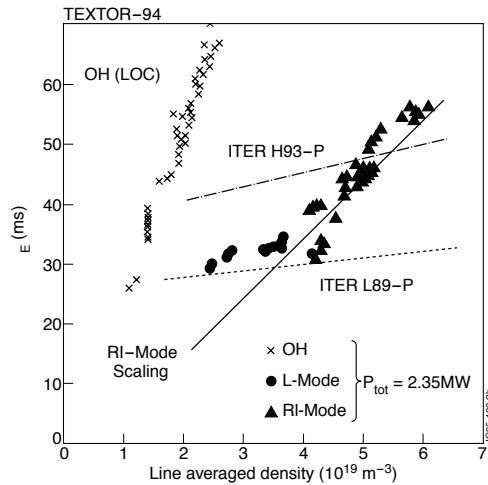


Fig. 2b: Same as Fig. 2a but with experimental results from TEXTOR-94 pertaining to OH (LOC), L-mode and RI-mode conditions ( $I_p = 350kA$ ,  $B_t = 2.25T$ ,  $P_{tot}$  (for L and RI-Mode) = 2.35 MW).

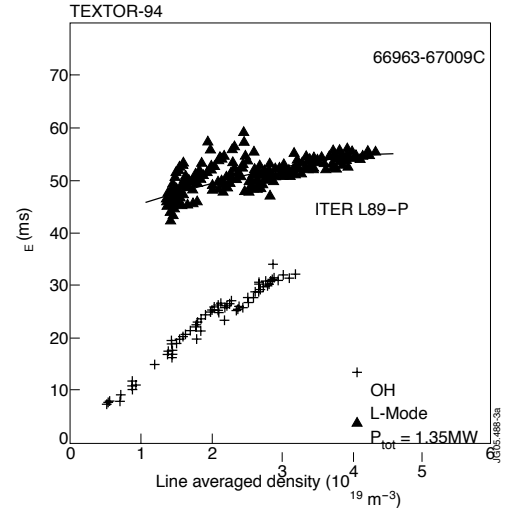


Fig. 3a: Plasma energy as a function of central line averaged density  $\bar{n}_{e0}$  for OH (LOC + start of SOC) and neutral beam heated discharges (L-Mode compared to the ITER L89-P scaling).

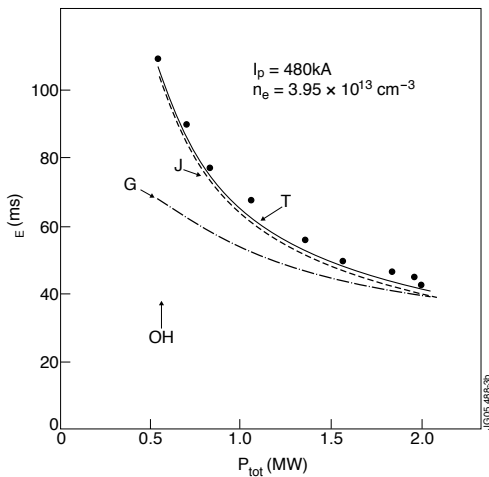


Fig. 3b: Confinement time degradation with  $P_{tot}$ . Comparison with L-mode scalings (G and K-G) and linear offset scalings (J and T) [6].

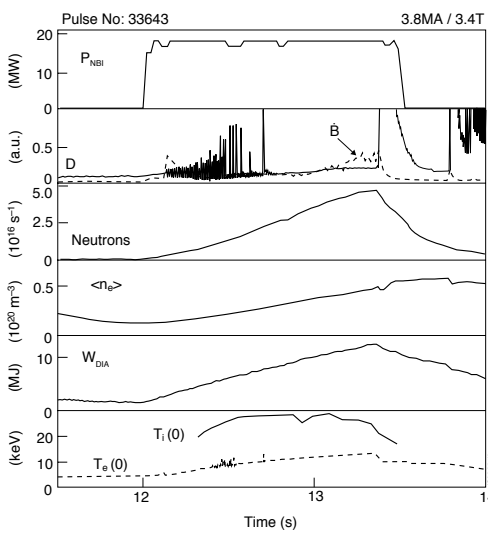


Fig. 4a: Hot ion H-mode discharge in JET. The D signal shows the occurrence of the ELM's. Between  $t = 12.7$  s and  $t = 13.4$  s there is an ELM-free period which ends with the onset of MHD turbulence followed by a giant ELM. During this phase there is a continuous increase of density, energy and neutron yield, which

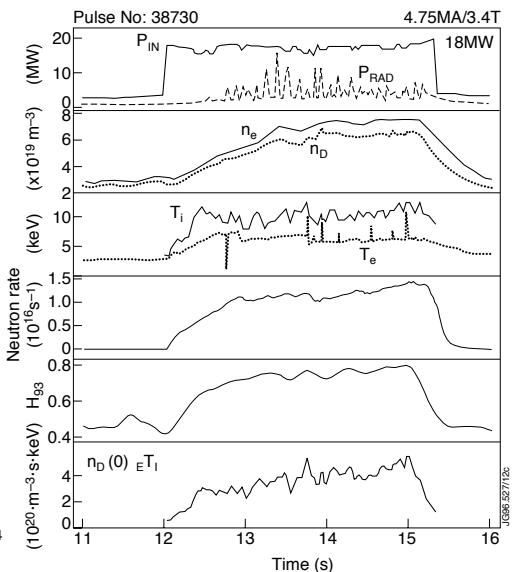


Fig. 4b: Steady-state ELMy H-Mode in JET with ITER-like core plasma conditions. Note the value reached by  $NT$  and  $f_{H93}$ . Also  $\bar{n}_{e0}/\bar{n}_{CR} \sim 0.75$

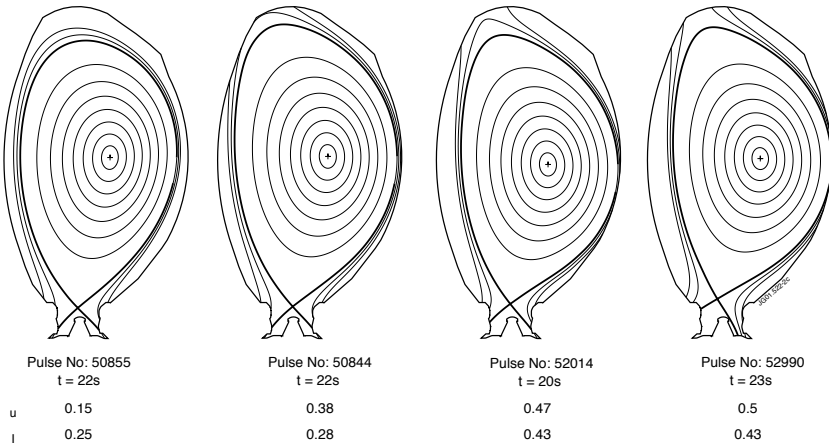


Fig 4c Different shapes for the plasma cross section which can be realised in JET. From left to right the average triangularity is increasing.

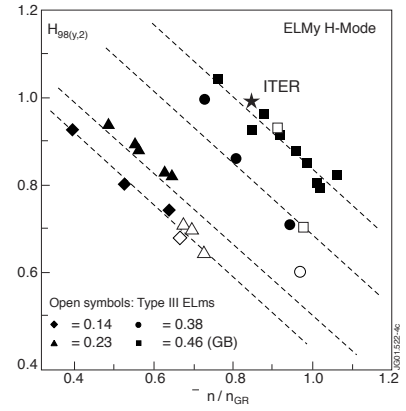


Fig 4d Confinement ( $H_{98(y,2)}$ ) versus the Greenwald factor ( $n/n_{GW}$ ) for different triangularities. For each triangularity with increasing density confinement degrades. However, increasing triangularity helps to increase confinement for a given density. For the highest triangularities the ITER values are reached.

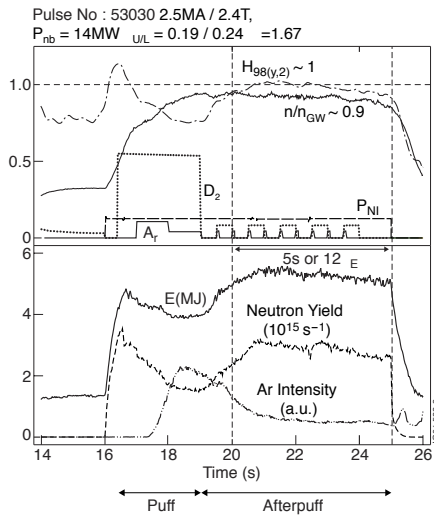


Fig 4e Example of a discharge obtained at JET with impurity seeding in a plasma with triangularity. In the afterpuff phase high density ( $n/n_{GW} = 0.9$ ) and high confinement ( $H_{98(y,2)} = 1.0$ ) is realised.

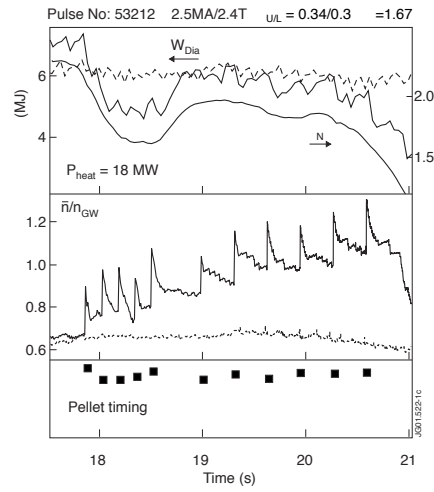


Fig 4f Example of a discharge with an adapted pellet fuelling rate. The dashed lines correspond to a reference discharge without pellet fuelling (and without gas puffing). The black squares indicate the pellet timing. In the second part of the fuelling rate (at an injection frequency of 6 Hz) high density is realised above the Greenwald limit with good confinement as seen from the diamagnetic energy and beta values.

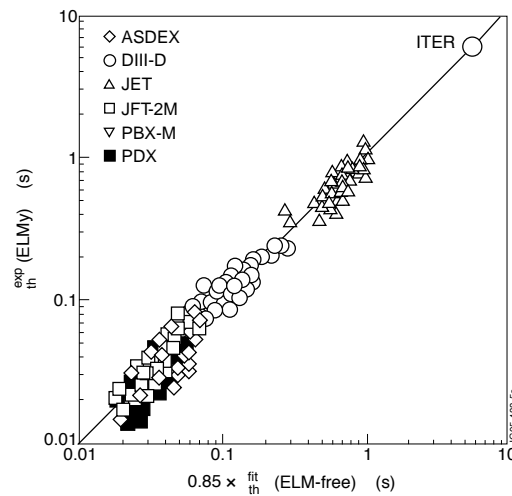


Fig. 5 Experiment confinement time (for thermal energy confinement) as a function of  $0.85 \times \tau_{th}^{fit}$  for different divertor machines. The needed extrapolation to ITER is also shown (corresponding to  $\tau_{th} = 6.1s$  and  $\bar{n}_{e0} = 1.3 \cdot 10^{20} m^{-3}$  and  $P_{tot} = 190 MW$ ). Note that if  $\tau_{th}$  is lower by 30%, no ignition takes place and  $Q = 10$ .

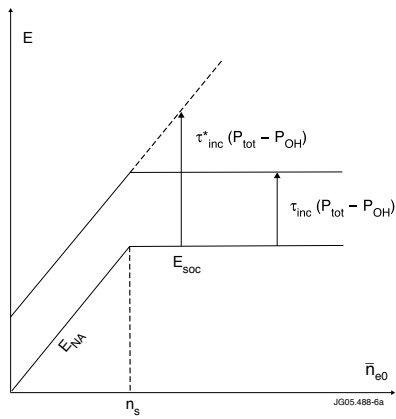


Fig. 6a: Schematic representation of the behaviour of the plasma energy content as a function of density, for discharges with ohmic and additional heating.

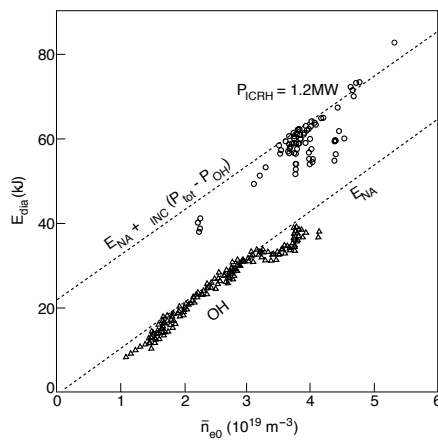


Fig. 6b: Corresponding experimental points of TEXTOR for ohmic discharges (where the start of the SOC regime appears) and for ICRH discharges in presence of Neon injection at  $I_p = 350$  kA.

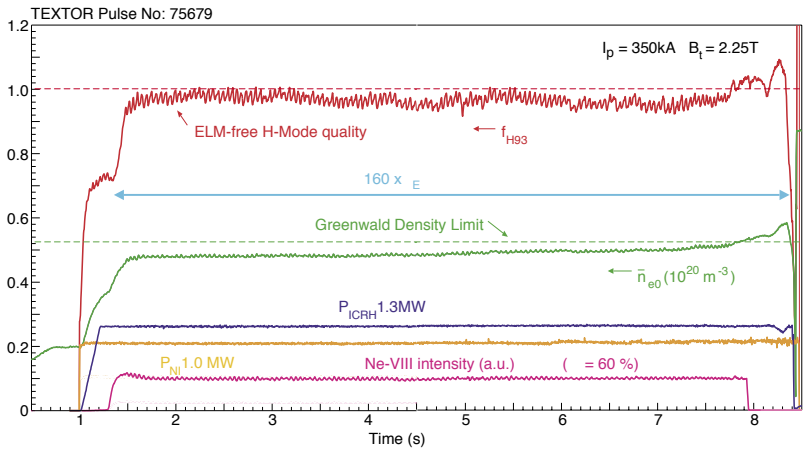


Fig. 7: Long stationary RI-mode discharge obtained with Ne seeding ( $I_p = 350$  kA,  $B_t = 2.25$  T). Shown are as the diamagnetic energy measurement, line average density  $\bar{n}_{e0}$ , P(NJ) (co-injection), P(ICRH), the Greenwald density limit and  $f_{H93}$  versus time.

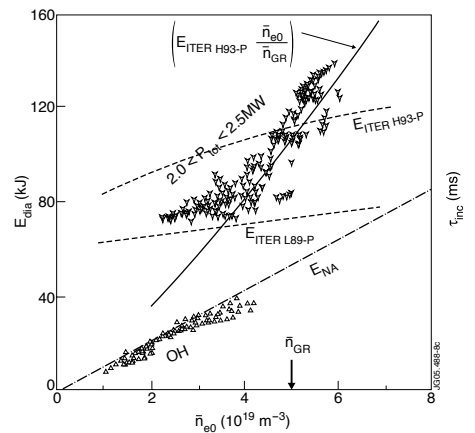


Fig. 8: Plasma energy as a function of the density  $\bar{n}_{e0}$  for ohmic discharges and for additionally heated ones (the latter in presence of Neon seeding and with  $2 < P_{tot} < 2.5$  MW). The predictions of the Neo-Alcator, ITER L89-P and  $(\bar{n}_{e0}/\bar{n}_{e0,GR}) \times$  ITER H93-P scalings are also indicated together with the value of the Greenwald limit.

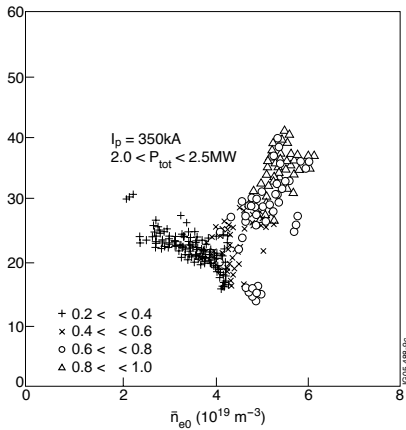
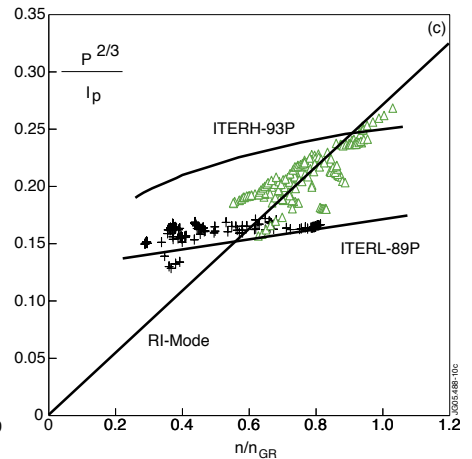
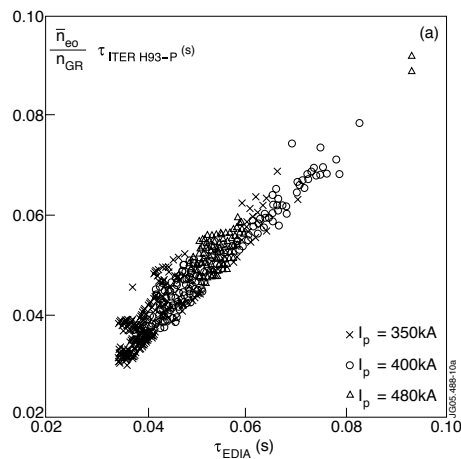
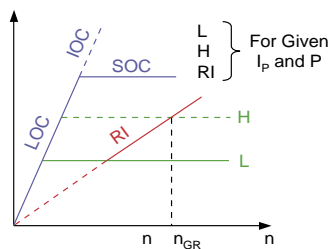


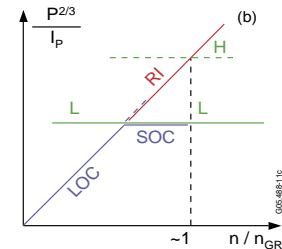
Fig. 9: Incremental confinement time versus  $\bar{n}_{e0}$  for the additionally heated discharges shown in Fig. 8. The corresponding values are indicated.



SCHMATIC CONFINEMENT BEHAVIOUR IN TEXTOR



$$\begin{aligned} \text{LOC} & n f(I_p) \quad n P_{OH}^{-2/3} \\ \text{L} & H \quad I_p P^{-2/3} \\ \text{SOC} & L \quad (P = P_{OH}) \end{aligned}$$



$$RI = \begin{cases} c^t n P^{-2/3} \\ \frac{n}{n_{GR}} \quad \text{ITER H93-P} \end{cases}$$

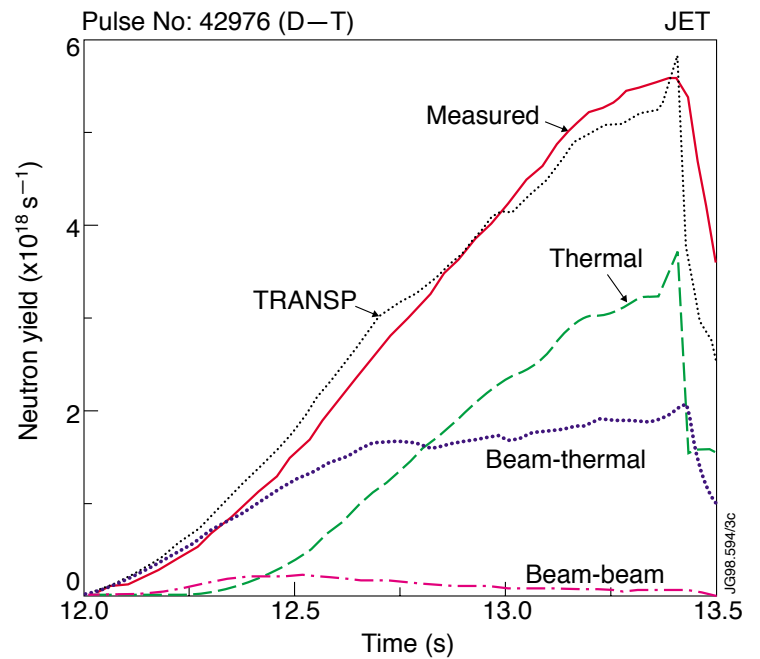
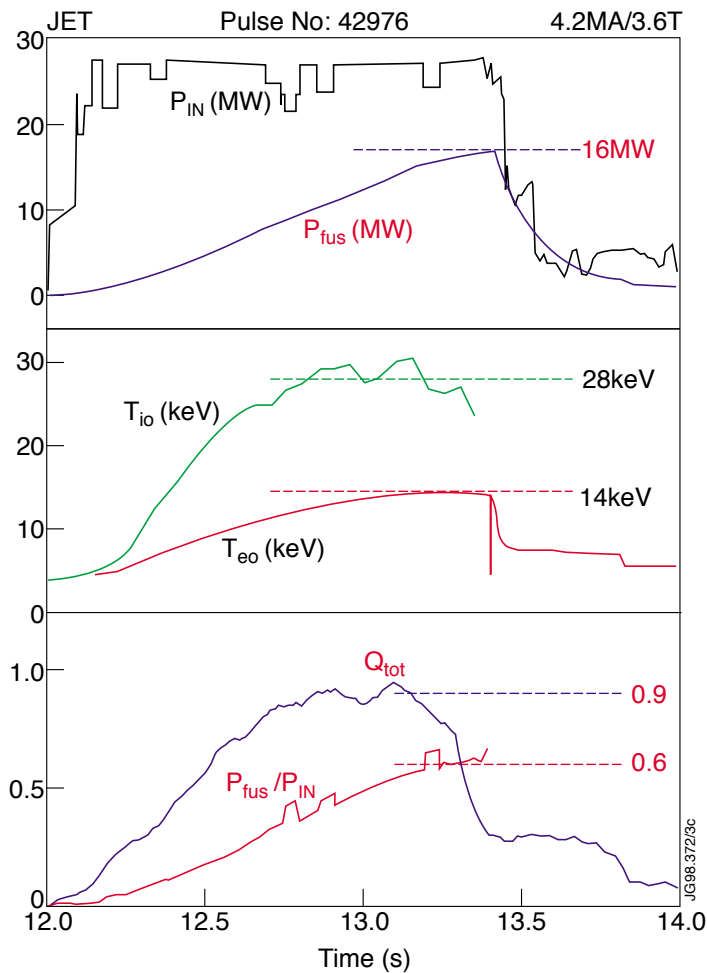
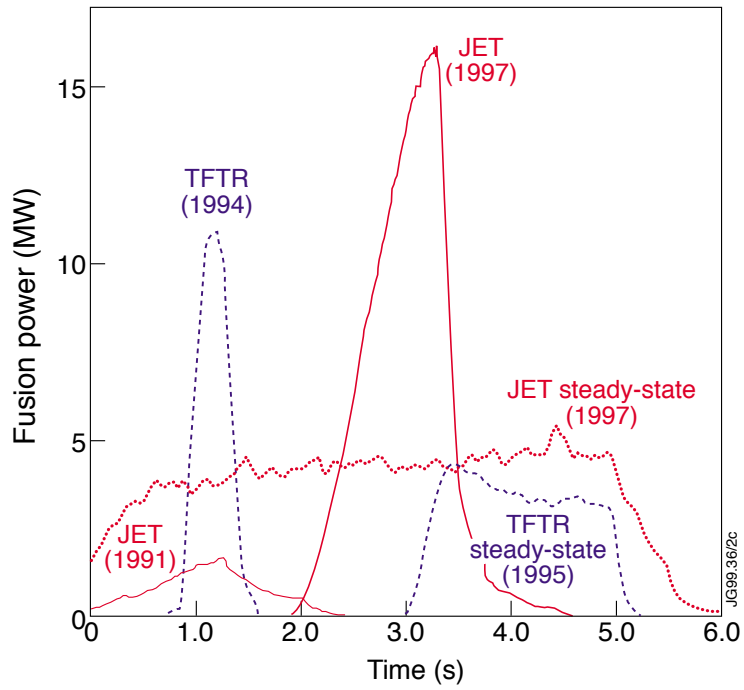


Fig. 11a): Fusion power development in the D-T campaigns of JET and TFTR. (I) Hot-ion modes, (II) Optimised shear and (III) steady-state ELMy H-Modes. b) Time traces of the highest performance JET D-T hot-ion H-Mode discharge producing a record fusion output of 16 MW and  $Q = 0.62$ . c) Time evolution of the observed total neutron yield compared with a simulation by the TRANSP code for the shot of Fig. 11b. Also shown are the thermal, beam-thermal and beam-beam contribution to the neutron yield as predicted by TRANSP.

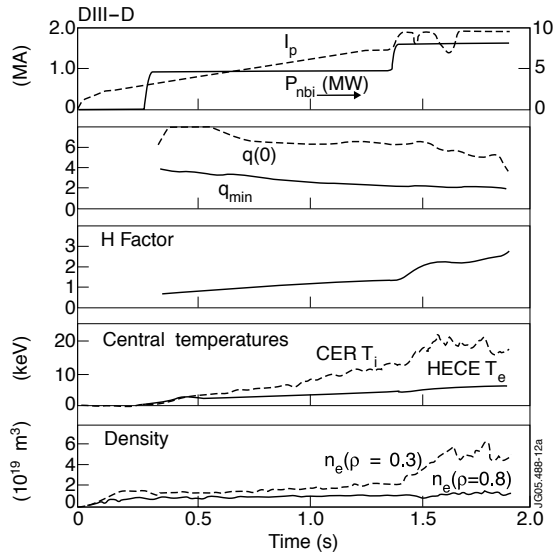


Fig. 12a: Discharge in DIII-D with early heating during the current ramping to the formation of an ITB. Shown versus time are  $I_p$ ,  $P_{NBI}$ ,  $q(0)$  and the off-axis minimum  $q$  value  $q_{min}$ , the enhancement factor  $H$  with respect to the L-mode scaling (ITER L89P), the central ion and electron temperatures and the density at two locations of  $r/a$ . [24]

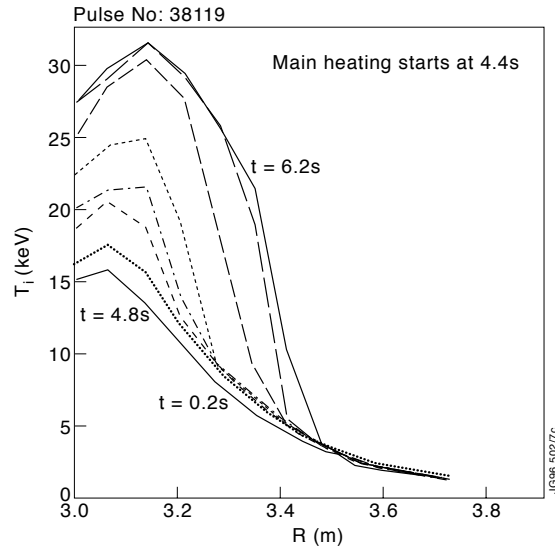


Fig. 12b: Evolution of the ion temperature profile in JET after the formation of an ITB (at  $R = 3.5m$ ) due to an early heating scenario (of NBI + ICRH).

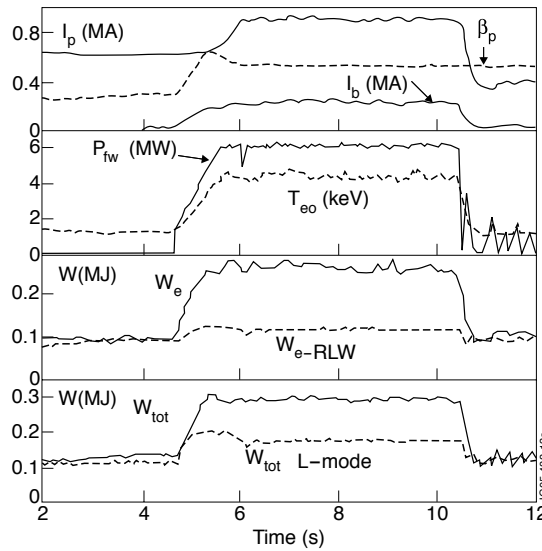


Fig. 13a: Stationary high bootstrap current discharge obtained by ICRH (fast wave electron heating scenario).  $I_b$  is the bootstrap current,  $P_{fw}$  the ICRH power,  $W_e$  and  $W_{tot}$  correspond to the electron and total plasma energies [25].  $W_{e-RLW}$  and  $W_{tot L-mode}$  are predictions of L-mode scalings

